JMSAE Journal of Materials Science and Applied Energy

Journal of Materials Science and Applied Energy

Journal home page: jmsae.snru.ac.th

Photon Interaction, Buildup Factors and Fast Neutron Removal of Some Scintillators Used X–Ray and CT Imaging

Kittisak Sriwongsa[a, b, *], Thanaboon Rimdusit[b], Jirayut Phothawilkiat[b], Suphaphit Ngampring[c], Thatchapol Hudsathapun[c], Punsak Glumglomchit[c], Sunantasak Ravangvong[d]

[a] *Lecturers responsible for Bachelor of Education Program in Physics, Faculty of Education, Silpakorn University, Nakhon Pathom, 73000 Thailand*

[b] *The demonstration school of Silpakorn University, Nakhon Pathom, 73000 Thailand*

[c] *Huahin Vitthayalai School, Hua–Hin, Prachuap Khiri Khan, 77110 Thailand*

[d] *Division of Science and Technology, Faculty of Science and Technology, Phetchaburi Rajabhat University, Phetchaburi, 76000 Thailand*

*Corresponding Author: sriwongsa_k@silpakorn.edu

Received 10 October 2020; **Revised** 6 November 2020; **Accepted** 19 April 2021; **Available online:** 1 May 2021

Abstract

Photon and neutron shielding properties for scintillators used X–ray and CT imaging to investigate in this paper. Photon shielding properties of scintillators were investigated by computation for mass attenuation coefficient (μ_m), effective atomic number (Z_{eff}), effective electron density (N_{el}) and mean free path (*MFP*) in the photon energy range 1 keV – 100 GeV, and buildup factor (BFs) were computed in photon energy region 15 keV – 15 MeV up to penetration depth of 40 *MFP* by Geometric progression (G–P) fitting formula. Lastly, removal cross–section for fast neutron (Σ_R) of scintillators were computed. The obtained results of some scintillators were compared, in terms of mass attenuation coefficient and mean free path with standard radiation shielding concretes. The results showed that the select scintillators better radiation shielding properties than the standard shielding concrete that can be developed as photon and neutron shielding materials.

Keywords: Scintillator; Radiation Shielding; Fast Neutron

Introduction

Today, radiation isotopes were used in many sectors such as agriculture and medicine whereas these sources are very dangerous which is including human life and sensitive laboratory device [1]. In the part of physics radiation, the attenuation of intensity radiation depends on the probability of interaction with the medium. These interactions are very important and can be discussed in the mass attenuation coefficient (μ_m) value. μ_m value is basic quantity was used determined and explained the other values about the penetration of radiation in a medium such as the effective atomic number (Z_{eff}), effective electron density (N_{el}), mean free path (*MFP*) and

buildup factors (*BFs*) [2, 3]. The probability of interaction with medium will higher when elements of the medium had a large atomic number and density, so, the choosing medium used to shield radiation should be selected medium as high atomic number and density elements [4 – 6].

Scintillator, one of material which absorbs radiation, high atomic number and density [7] and used in several applications such as medical imaging, the technology of astrophysical and space, nuclear fusion devices [8 – 11]. The utilization scintillator for radiation shielding and neutron is important which could be considered the basic value to discuss the penetration of radiation in a medium such as mass attenuation coefficient (μ_m), effective atomic number (Z_{eff}), effective electron density (N_{el}), half value layer (*HVL*) and build up factors (*BFs*) as mentioned before [12]. Gadolinium oxide (Gd_2O_3) has properties such as high thermal and chemical stability, low phonon energy, non-toxicity, high refractive index, non–hygroscopic nature, high dielectric constant and high bandgap [13] and gadolinium oxysulfide (Gd_2OS) has properties such as hard radiation stability, high X–ray absorption and high density makes it an effective trap of the incident X–ray photon [14] while gadolinium orthosilicate (Gd_2SiO_5: GSO) has high density, relatively fast decay time and high light output [15]. These properties of scintillators were according the properties of radiation shielding materials.

In this context was computed μ_m, Z_{eff}, N_{el} and *MFP* value at photon energy ranging 1 keV – 100 GeV by WinXCOM software program while energy absorption buildup factors (*EABF*) and exposure buildup factors (*EBF*) of scintillator was computed at photon energy ranging 15 keV – 15 MeV by using G-P fitting method. Finally, to evaluate effective removal cross–sections values (Σ_R) which presented neutron protection efficiency of scintillators.

Theories and Computation Method

Scintillator

Scintillator is inorganic material and used in field of ionizing nuclear radiation detection. To develop scintillator materials for radiation shield, the knowledge of radiation shielding parameters are very important for developed scintillators using against radiation such as μ_m value due to this value show probability of interaction. In addition, when radiation interacts with medium, Z_{eff}, N_{el}, *MFP*, EABF and EBF are basic values required to discuss the penetration of radiation in medium [12].

Radiation Shielding Properties

The mass attenuation coefficient (μ_m) of scintillators was calculated theoretically by using mixture rule and WinXCOM software program [16, 17] as shown in equation (1);

$$\mu_m = \sum_{i=1}^{n} w_i \mu_{mi} \tag{1}$$

At this point, w_i and μ_{mi} are weight fraction and mass attenuation coefficients of constituent elements, respectively. Using μ_m value from equation (1) calculated Z_{eff} and N_{el} [18 – 20] as shown in equation (2) and (3);

$$Z_{eff} = \frac{\sigma_{t,a}}{\sigma_{t,el}} \tag{2}$$

$$N_{el} = \frac{Z_{eff} N_A}{M} \sum_i n_i \tag{3}$$

Effective atomic cross–section ($\sigma_{t,a}$) were computed by equation (4);

$$\sigma_{t,a} = \frac{\sigma_t}{\sum_i n_i} \tag{4}$$

The total interaction cross–section (σ_t) of scintillators have been computed with helped of μ_m and estimated by equation (5);

$$\sigma_t = \frac{M \mu_m}{N_A} a \tag{5}$$

Total electron cross–section ($\sigma_{t,el}$) were determined by equation (6);

$$\sigma_{t,el} = \frac{1}{N_A} \sum_i \frac{f_i A_i}{Z_i} (\mu_m)_i \tag{6}$$

At this point $\sigma_{t,a}$, σ_t and $\sigma_{t,el}$ are effective atomic cross-section, total photon interaction cross-section, and electronic cross-section, respectively. M is molecular weight, N_A is Avogadro's number, n_i is the number of formula units of the molecule, A_i indicates atomic weight of element i, f_i presents a fractional abundance of constituent element and Z_i is an atomic number of element i. Mean free path (*MFP*) of scintillators was evaluated by using linear attenuation coefficient (μ) [18, 19] as shown in equation (7);

$$MFP = \frac{1}{\mu} \tag{7}$$

Build–Up Factors (*BFs*)

The BFs are basically value used design medium for radiation shielding. BFs separated two types, 1) EABF and 2) EBF obtained by computing from Geometrical Progression (G–P) fitting method in energy region 15keV–15 MeV and these values can be following equation (8) – (9). Firstly, it is very important to know that the equivalent atomic number (Z_{eq}) values must lie at specific energy between Z_1 and Z_2 atomic numbers ($Z_1 < Z_{eq} < Z_2$) [21, 22] as shown in equation (8) – (9);

$$B(E,x) = 1 + \frac{b-1}{K-1}(K^x - 1), K \neq 1 \tag{8}$$

$$B(E,x) = 1 + (b-1)x, K = 1a \tag{9}$$

Herewith K (E, x), photon dose multiplication factor, b, build–up factor corresponding to 1 *MFP* which obtained from equation (10);

$$K(E,x) = cx^a + d\frac{\tanh\left(\frac{x}{x_k} - 2\right) - \tanh(-2)}{1 - \tanh(-2)}, x \leq 40MFP \tag{10}$$

Lastly, fast neutrons removal cross-sections (Σ_R) for scintillators [19, 22] can be computed using the following equation (11) and (12);

$$\sum\nolimits_{\frac{R}{\rho}} = \sum_i w_i \left(\sum\nolimits_{\frac{R}{\rho}} \right) \tag{11}$$

$$\sum\nolimits_R = \sum\nolimits_i \rho_i \left(\sum\nolimits_{\frac{R}{\rho}} \right)_i \tag{12}$$

Where ρ_i is partial density and $\Sigma_{R/\rho}$ are partial density and mass removal cross-section of ith element, respectively.

Results and Discussion

The samples and properties of some scintillators are listed in Table1. The μ_m, Z_{eff}, N_{el} and *MFP* versus energy for some scintillators were presented in Fig. 1, 2, 3, and 4, respectively. The EABF and EBF values of some scintillators versus energy are presented in Fig. 6 and 7 (a) – (c) for different deep penetration at 1, 5, 10, 15, 20, 30, and 40 *MFP*. The EABF and EBF values for some scintillators versus deep penetration at energy 0.015, 0.15, 1.50, 3, 8, and 15 MeV are presented in Fig. 8 and 9 (a) – (d). Lastly, fast neutrons removal cross-sections (Σ_R) for scintillators are shown in Fig. 9.

Table 1 Properties of some scintillators used X–ray and CT imaging.

Sample	Density (g cc^{-1})	Ref.
$Gd_2O_3:Eu^{3+}$	7.55	[11]
Gd_2O_2S:Pe,Ce,F	7.34	[11]
GSO:Ce	6.70	[11]

μ_m, Z_{eff}, N_{el} and MFP of Scintillators

The μ_m versus photon energy at 1 keV–100 GeV of scintillators is presented in Fig. 1. From Fig. 1 μ_m values of all scintillators are decrease exponentially with increasing photon energies. At low energy, μ_m values are very high and decrease quickly with increasing energies. At intermediate energy, μ_m values are slow rate and becoming approximately constant at high energy. These events were discussed on the photoelectric effect, Compton scattering and pair production which appear and dominate at low, intermediate and high energy, respectively. From Fig. 1 graph are not continuous because of absorption edges of elements as presented in Table 2 and Gd_2O_3 scintillator has higher μ_m than other scintillators as indicated that Gd_2O_3 was used radiation shielding better other scintillators.

Table 2 Absorption edges (keV) of elements.

Element	K	L1	L2	L3	M1	M2	M3	M4	M5
Si	1.839	-	-	-	-	-	-	-	-
S	2.472	-	-	-	-	-	-	-	-
Gd	50.24	8.38	7.93	7.24	1.88	1.69	1.54	1.22	1.19

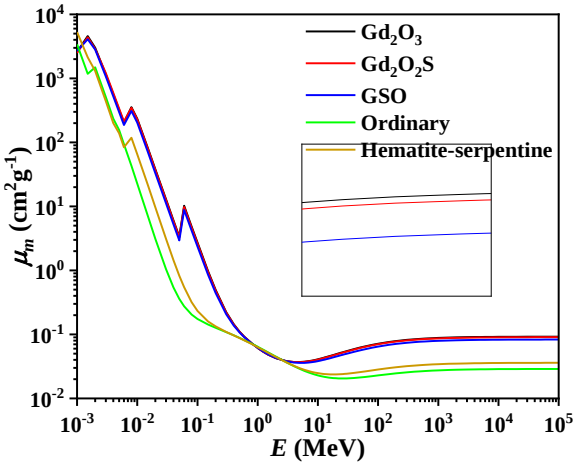

Fig. 1 μ_m versus photon energy.

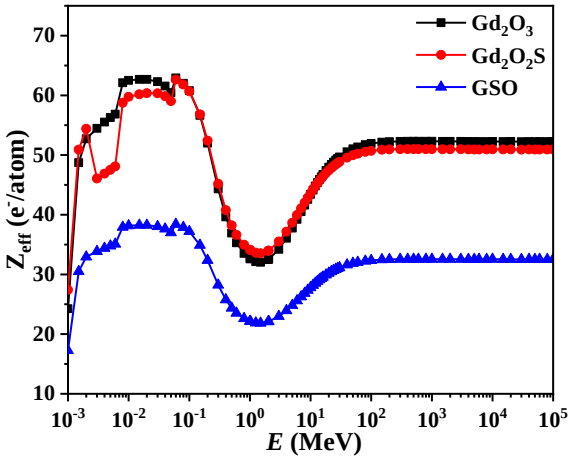

Fig. 2 Z_{eff} versus photon energy.

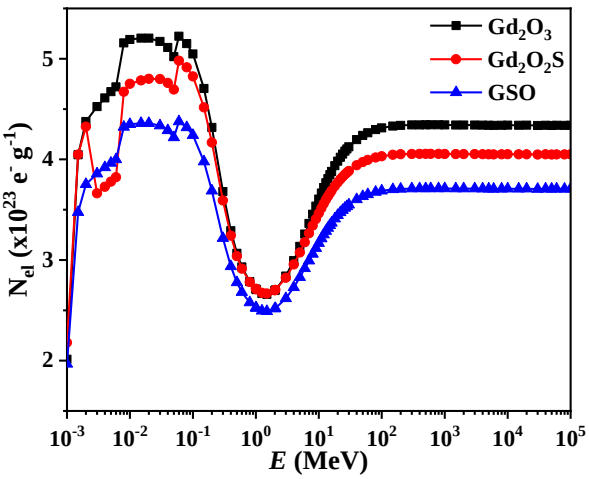

Fig. 3 N_{el} versus photon energy.

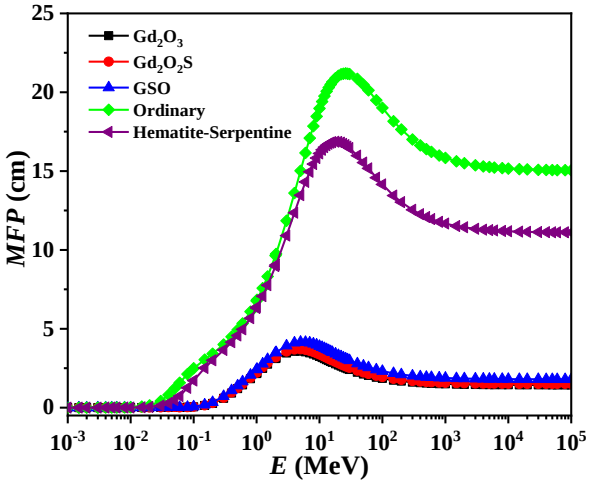

Fig. 4 *MFP* versus photon energy.

The Z_{eff} versus photon energy for scintillators has been presented in Fig. 2. It has been observed in Z_{eff} because of the main of different photon interaction processes. At lower energies, the photoelectric effect is the main photon interaction. When energy is adjacent to K-absorption edges of each element (Si, S, Gd) existent in scintillators, Z_{eff} values sudden shift like μ_m which indicates that correspond to elements K-absorption edge. This mechanism is main below 0.10 MeV. Hence, this event is computed by Z dependence of total atomic cross-sections and high Z elements from cross-section of the photoelectric absorption process. At intermediate energy ranging, the main interaction is Compton scattering, Z_{eff} value of scintillators was found the lowest. And then at high energy ranging which pair production is main interaction, Z_{eff} value increases again. At energy more than over about 100 MeV, Z_{eff} value nearly constant, this is discussing from cross-section of which possesses a weaker Z^2 dependence. However, cross-section of Compton scattering depends on Z whereas less than the photoelectric absorption and pair production process. The N_{el} value has the same trend of Z_{eff} that indicates the behavior of N_{el} like Z_{eff} as shown in Fig.3.

The *MFP* value for c scintillators are exhibited in Fig. 4. As indicated *MFP* value increase with increasing energy while GSO and Gd_2O_3 have the highest and lowest *MFP*, respectively. This results from the density of scintillators which high density presented radiation absorption efficiency of scintillator. Gd_2O_3 has the highest density, thus the density of scintillator plays an important role in affecting photon attenuation. Since Gd_2O_3 has the lowest *MFP* at the same energy, so Gd_2O_3 is required a small thickness when compared with the other scintillator and used for radiation shielding.

EABF, EBF and Σ_R of Scintillators

EABF and EBF of scintillators have been explained depending on density, photon energy, and deep penetration. Fig. 5 shows Z_{eq} of scintillators versus photon energy. It is clearly seen that Gd_2O_3 scintillator has the highest Z_{eq} values.

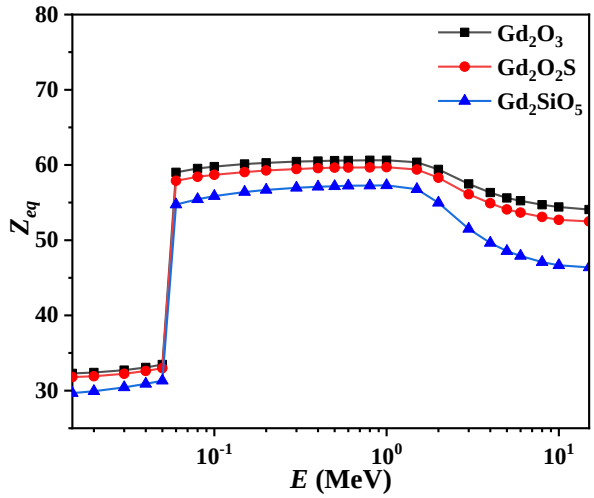

Fig. 5 Z_{eq} versus photon energy.

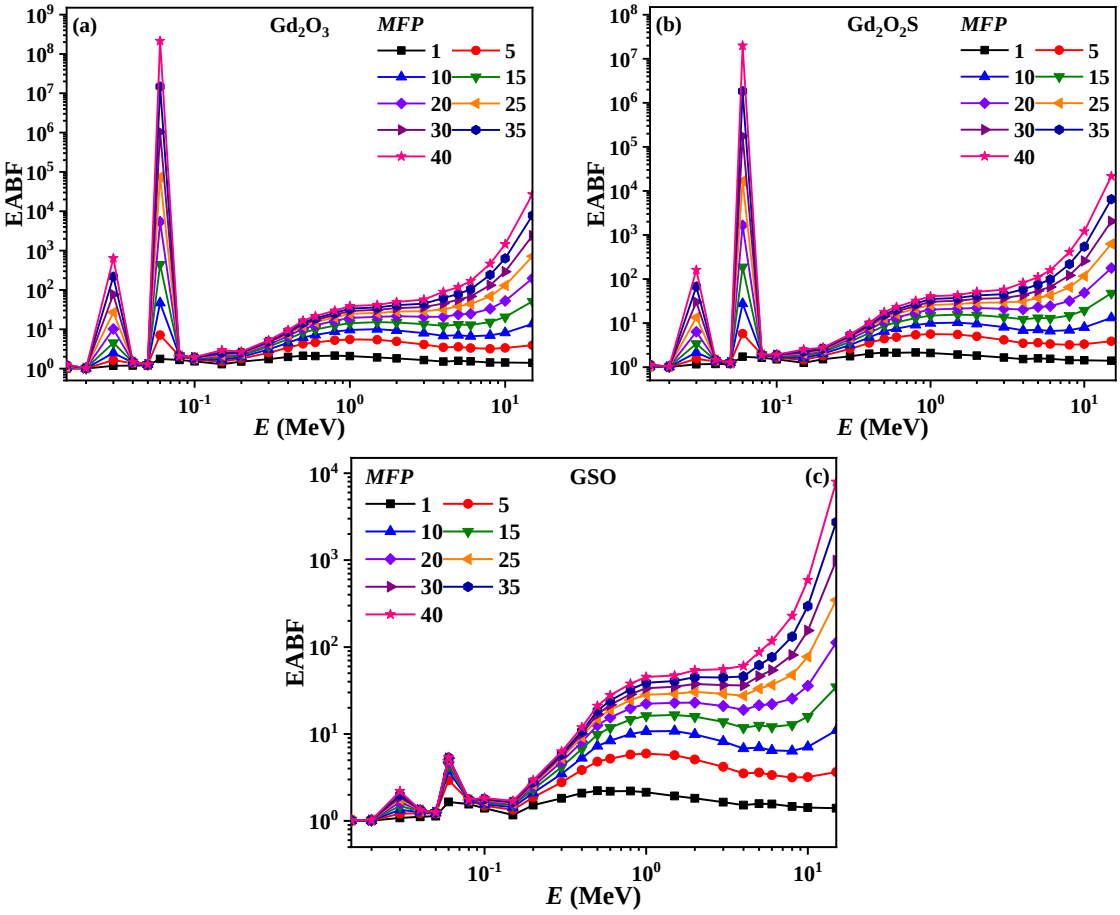

Fig. 6 EABF versus photon energy at 1, 5, 10, 15, 20, 25, 30, 35, and 40 *MFP* of (a) Gd_2O_3, (b) Gd_2O_2S, and (c) GSO.

The EABF and EBF, with energy, for all scintillators at different deep penetration, have been exhibited in Fig. 6 and 7(a) – (c), respectively. These figures, EABF and EBF values for all scintillators increase with increasing photon energy and the maximum values indicated that EABF and EABF are dependent on deep penetration and composition of scintillators. These events can be discussed on the important interaction. At low energy ranging, values of EABF and EBF are smallest because of photons were completely absorbed and the main interaction process is the photoelectric effect. At intermediate energy ranging, the values of EABF and EBF are highest because of Compton scattering is the main interaction process. At high energy ranging, pair production is main interaction, photons have been absorbed again. The EABF and EBF results of scintillators have two sharp peaks at 40 and 60 keV which may be due to K-absorption edges of elements. The highest EABF and EBF values were found at 40 *MFP* deep penetration while the lowest values were found at 1 *MFP* this because of multiple scatterings were occurred at high deep penetration.

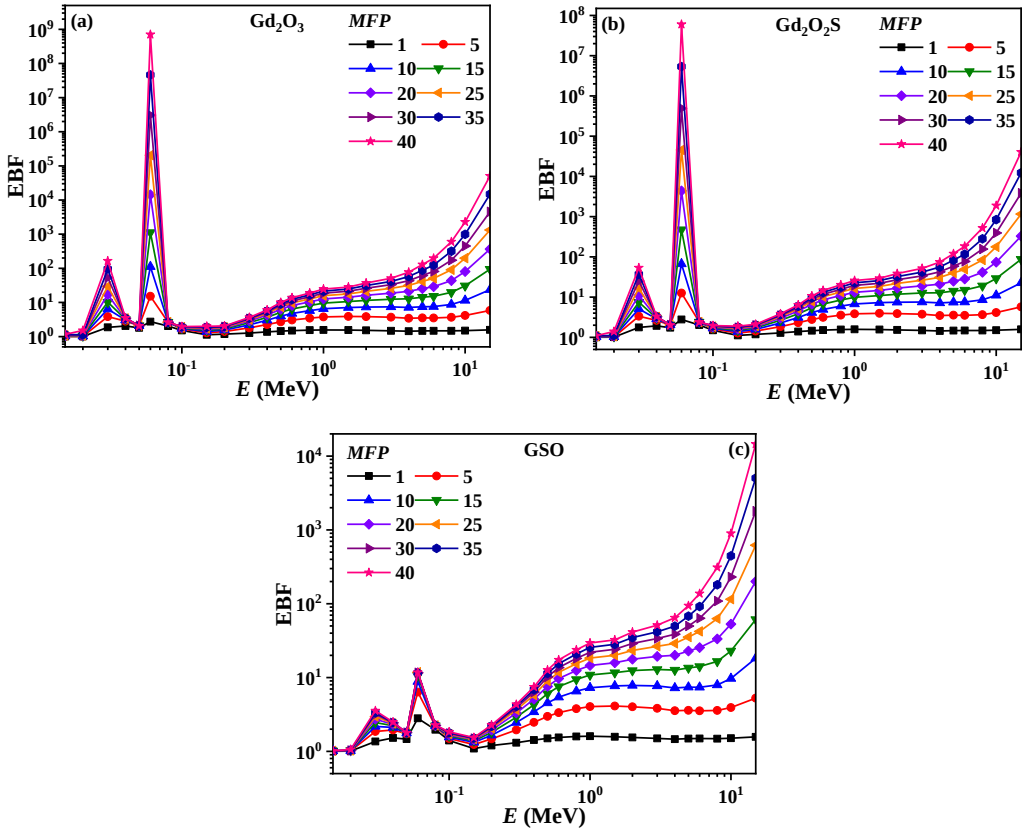

Fig. 7 EBF versus photon energy at 1, 5, 10, 15, 20, 25, 30, 35, and 40 *MFP* of (a) Gd_2O_3, (b) Gd_2O_2S, and (c) GSO.

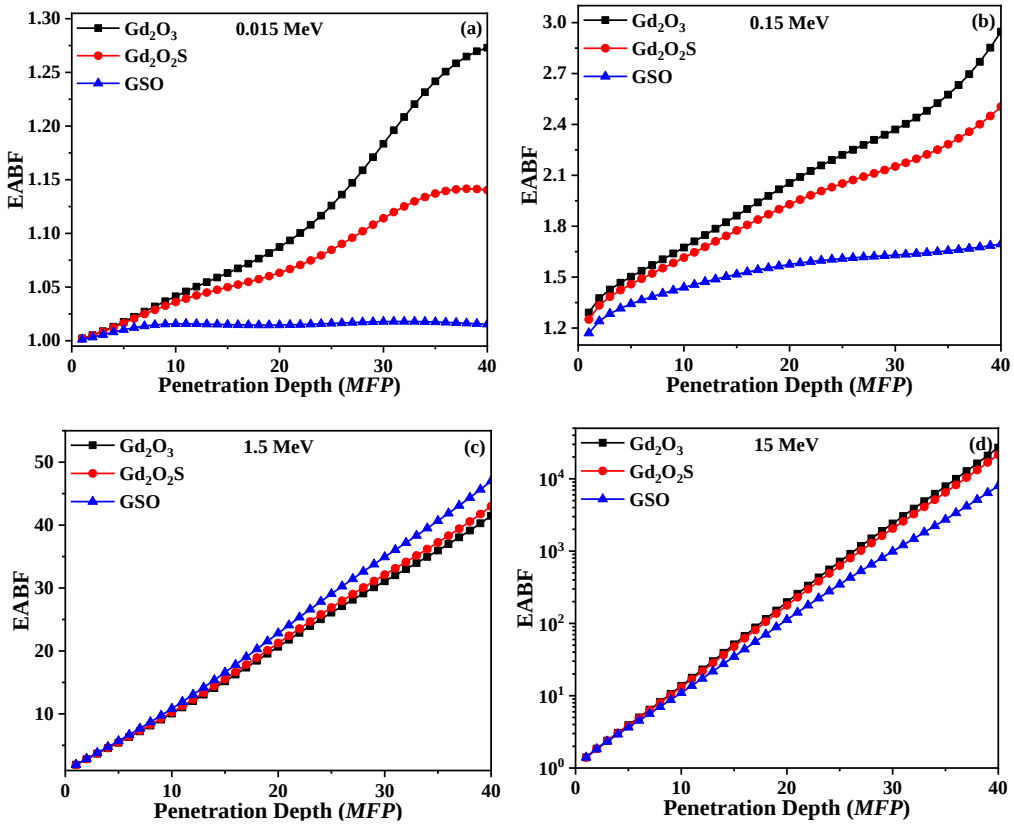

Fig. 8 EABF versus deep penetration for (a) 0.015 MeV, (b) 0.15MeV, (c) 1.50 MeV and (d) 15 MeV.

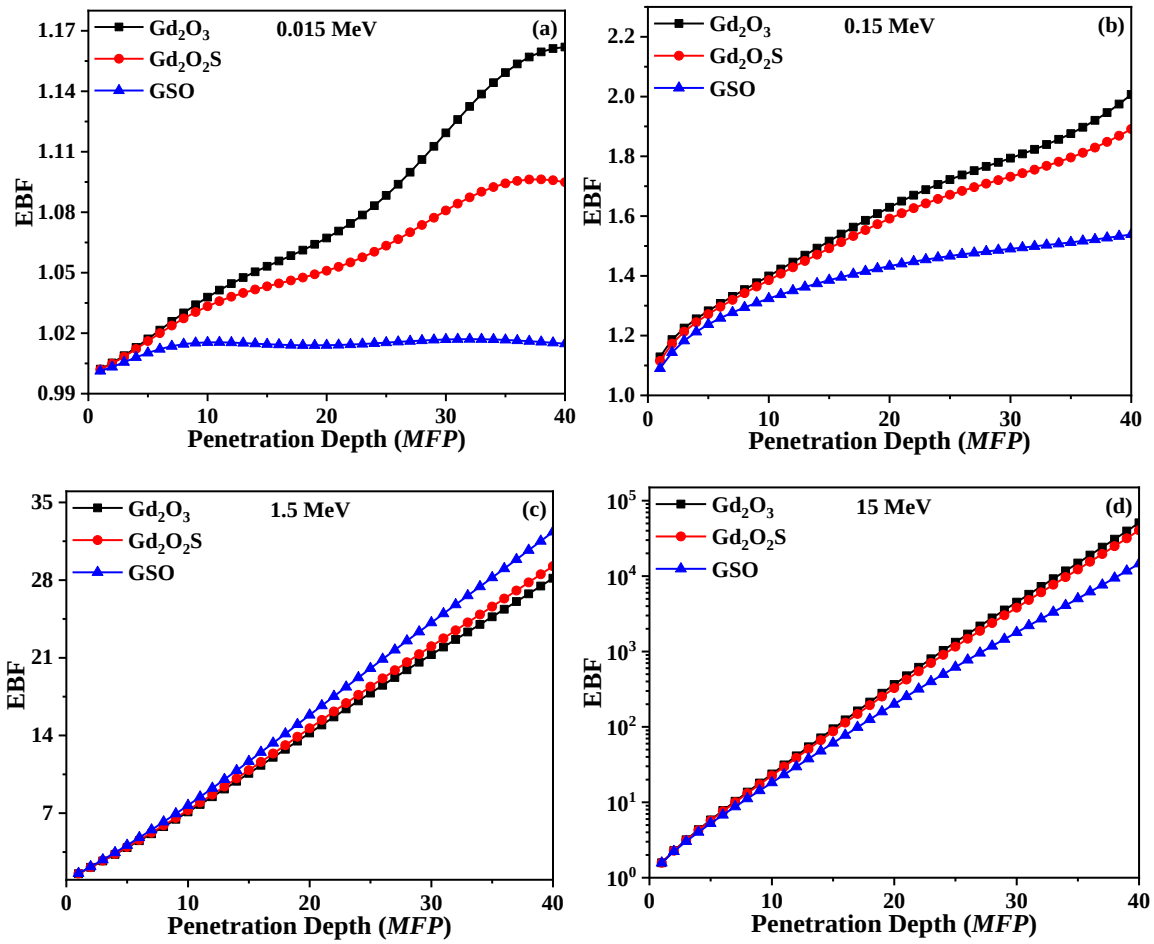

Fig. 9 EBF versus deep penetration for (a) 0.015 MeV, (b) 0.15 MeV, (c) 1.50 MeV, and (d) 15 MeV.

The EABF and EBF, with deep penetration, for all scintillators at energy 0.015, 0.15, 1.50, and 15 MeV have been exhibited in Fig 8, and 9 (a) – (d), respectively. It can be noted that EABF and EBF value of scintillators increase with increasing energy and deep penetration. These events can be discussed on the basic of the partial photon interaction process. At low, intermediate and high energy ranging, photoelectric effect, Compton scattering, and pair production is the main interaction, respectively. At energy 0.015 and 0.15 MeV, EABF and EBF of Gd_2O_3 value presented maximum values. This indicates that at low energies, EABF and EBF depend clearly on the chemical composition of scintillators. At 15 MeV energy, Gd_2O_3 showed the largest EABF and EBF again that because of pair/triplet production in scintillators which generates electron/positron pair. This process becomes to allow photon to accumulate in Gd_2O_3.

The removal cross-section for fast neutron (Σ_R) of scintillators is presented in Fig. 8. The highest Σ_R (cm^{-1}) value was found for GSO, this reveals that low-*Z* elements are not only responsible for neutron removal but also including of low and high-*Z* elements [23].

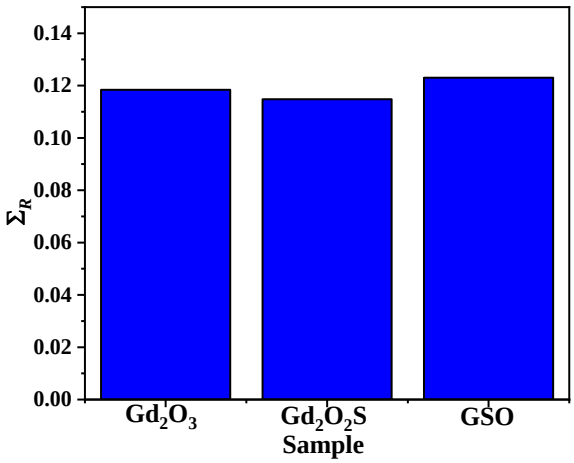

Fig. 10 Σ_R of scintillators.

Conclusion

In this context, scintillators used X–ray and CT imaging were estimated radiation shielding at photon energy ranging 1 keV – 100 GeV, buildup factors at photon energy range 15 keV – 15 MeV up to deep penetration of 40 *MFP*, and fast neutron removal cross–section. The simulated values find that Gd_2O_3 scintillator showed excellent radiation shielding because of the highest values for mass attenuation coefficient (μ_m), effective atomic number (Z_{eff}) and effective electron density (N_{el}) and lower values for mean free path (*MFP*) and buildup factors (*BFs*). While neutrons shielding, GSO scintillator showed excellent because of the highest removal cross–section for fast neutron (Σ_R) value. This study on the interaction of radiation and neutron with scintillators provides sufficient information for the selection of these scintillators for the design and applications of shielding materials in various applications.

Acknowledgement

This work was supported by the Ministry of Research and Technology - The Republic of Indonesia and the Indonesian Institute of sciences through the Mandiri research grant are greatly acknowledged.

References

[1] K. Kaur, K.J. Singh, V. Anand, Correlation of gamma ray shielding and structural properties of PbO–BaO–P_2O_5 glass system, Nucl. Eng. Des. 28 (2015) 31 – 38.

[2] M. Almatari, O. Agar, E.E. Altunsoy, O. Kilicoglu, M.I. Sayyed, H.O. Tekin, Photon and neutron shielding characteristics of samarium doped lead alumino borate glasses containing barium, lithium and zinc oxides determined at medical diagnostic energies, Results Phys. 12 (2019) 2123 – 2128.

[3] H.O. Tekin, E.E. Altunsoy, E. Kavaz, M.I. Sayyed, O. Agar, M. Kamislioglu, Photon and neutron shielding performance of boron phosphate glasses for diagnostic radiology facilities, Results Phys. 12 (2019) 1457 – 1464.

[4] O. Agar, M.I. Sayyed, H.O. Tekin, K.M. Kaky, S.O. Baki, I. Kityk, An investigation on shielding properties of BaO, MoO_3 and P_2O_5 based glasses using MCNPX code, Results Phys. 12 (2019) 629 – 634.

[5] N.J. AbuAlRoos, N.A.B. Amin, R. Zainon, Conventional and new lead–free radiation shielding materials for radiation protection in nuclear medicine: A review, Radiat. Phys. Chem. 165 (2019) 108439.

[6] M.I. Sayyed, H.O. Tekin, M.M. Taki, M.H.A. Mhareb, O. Agar, E. Şakar, K.M. Kaky, Bi_2O_3–B_2O_3–ZnO–BaO–Li_2O glass system for gamma ray shielding applications, Optik. 201 (2020) 163525.

[7] S. Jagtap, P. Chopade, S. Tadepalli, A. Bhalerao, S. Gosavi, A review on the progress of ZnSe as inorganic scintillator, Opto. -Electron Rev. 27 (2019) 90 – 103.

[8] J. Pejchal, J. Barta, T. Trojek, R. Kucerkova, A. Beitlerova, M. Nikl, Luminescence and scintillation properties of rare–earth–doped $LaAlO_3$ single crystals, Radiat. Meas. 121 (2019) 26 – 31.

[9] I. García–Cortés, M. Malo, A. Moroño, P. Muñoz, P. Valdivieso E. Hodgson, In–situ evaluation of radiation induced optical degradation of candidate scintillator materials for ITER's gamma and neutron detectors, Fusion Eng. Des. 136 (2018) 493 – 497.

[10] J. Oliveira, V. Correia, P. Costa, A. Francesko, G. Rocha, S. Lanceros–Mendez, Stretchable scintillator composites for indirect X-ray detectors, Compos. Part B. 133 (2018) 226 – 231.

[11] P. Lecoq, Development of new scintillators for medical applications, Nucl. Instrum. Meath. A. 809 (2016) 130 – 139.

[12] S.A.M. Issa, M.I. Sayyed, M.H.M. Zaid, K.A. Matori, A Comprehensive Study on Gamma Rays and Fast Neutron Sensing Properties of GAGOC and CMO Scintillators for Shielding Radiation Applications, J. Spectrosc. (2017) 1 – 9.

[13] R. Priya, O.P. Pandey, S.J. Dhoble, Review on the synthesis, structural and photo-physical properties of Gd_2O_3 phosphors for various luminescent applications, Opt. Laser. Technol. 135 (2021) 106663.

[14] A.A. Kharieky, K.R.E. Saraee, Synthesis and characterization of radio and thermoluminescence properties of Sm doped Gd_2O_3, Gd_2O_2S and $Gd_2O_2SO_4$ nanocrystalline phosphors, J. Lumin. 220 (2020) 116979.

[15] S. Okumura, S. Yamamoto, J.Y. Yeom, N. Shimura, H. Ishibashi, Precise timing resolution measurements of GSO scintillators with different Ce concentrations combined with silicon photomultipliers, Nucl. Instrum. Meth. A. 797 (2015) 153 – 157.

[16] H. Liu, J. Shi, H. Qu, D. Ding, An investigation on physical, mechanical, leaching and radiation shielding behaviors of barite concrete containing recycled cathode ray tube funnel glass aggregate, Constr. Build. Mater. 201 (2019) 818 – 827.

[17] S.A.M. Issa, M. Ahmad, H.O. Tekin, Y.B. Saddeek, M.I. Sayyed, Effect of Bi_2O_3 content on mechanical and nuclear radiation shielding properties of Bi_2O_3–MoO_3–B_2O_3–SiO_2–Na_2O–Fe_2O_3 glass system, Results Phys. 13 (2019) 102165.

[18] S.A.M. Issa, Y.B. Saddeek, M.I. Sayyed, H.O. Tekin, O. Kilicoglu, Radiation shielding features using MCNPX code and mechanical properties of the $PbO–Na_2O–B_2O_3–CaO–Al_2O_3–SiO_2$ glass systems, Compos. B. 167 (2019) 231 – 240.

[19] O. Kilicoglu, E.E. Altunsoy, O. Agar, M. Kamislioglu, M.I. Sayyed, H.O. Tekin, N. Tarhan, Synergistic effect of La_2O_3 on mass stopping power (MSP)/projected range (PR) and nuclear radiation shielding abilities of silicate glasses, Results Phys. 14 (2019) 102424.

[20] A. Kumar, Gamma ray shielding properties of $PbO–Li_2O–B_2O_3$ glasses, Radiat. Phys. Chem. 136 (2017) 50 – 53.

[21] B. Oto, N. Yıldız, T. Korkut, E. Kavaz, Neutron shielding qualities and gamma ray buildup factors of concretes containing limonite ore, Nucl Eng Des. 293 (2015) 166 – 175.

[22] M.I. Sayyed, H. Elhouichet, Variation of energy absorption and exposure buildup factors with incident photon energy and penetration depth for boro–tellurite ($B_2O_3–TeO_2$) glasses, Radiat. Phys. Chem. 130 (2017) 335 – 342.

[23] V.P. Singh, N.M. Badiger, N. Chanthima, J. Kaewkhao. Evaluation of gamma–ray exposure buildup factors and neutron shielding for bismuth borosilicate glasses, Radiat. Phys. Chem. 98 (2014) 14 – 21.